Nuclear Inst. and Methods in Physics Research, A 1050 (2023) 168119

Contents lists available at ScienceDirect

Nuclear Inst. and Methods in Physics Research, A

journal homepage: www.elsevier.com/locate/nima

Characterization of the polysilicon resistor in silicon strip sensors for ATLAS inner tracker as a function of temperature, pre- and post-irradiation

V. Latoňová [a,b,*], P.P. Allport [c], E. Bach [d], J. Bernabeu [e], A. Chisholm [c], V. Cindro [f], V. Fadeyev [g], P. Federičová [a], J. Fernandez-Tejero [h,i], W. George [c], L. Gonella [c], K. Hara [j], S. Hirose [j], T. Ishii [j], T. Knight [k], I. Kopsalis [c], J. Kroll [a], J. Kvasnička [a], C. Lacasta [e], J. Lomas [c], I. Mandić [f], M. Mikeštíková [a], R.S. Orr [k], E. Rossi [k], C. Solaz [e], U. Soldevila [e], M. Ullan [d], Y. Unno [l]

[a] *Academy of Sciences of the Czech Republic, Institute of Physics, Na Slovance 2, 18221 Prague 8, Czech Republic*
[b] *Faculty of Mathematics and Physics, Charles University, V Holesovickach 2, Prague, CZ18000, Czech Republic*
[c] *School of Physics and Astronomy, University of Birmingham, Birmingham B152TT, United Kingdom*
[d] *Centro Nacional de Microelectronica (IMB-CNM, CSIC), Campus UAB-Bellaterra, 08193 Barcelona, Spain*
[e] *Instituto de Física Corpuscular, IFIC/CSIC-UV, C/Catedrático José Beltrán 2, E-46980 Paterna, Valencia, Spain*
[f] *Experimental Particle Physics Department, Jožef Stefan Institute, Jamova 39, SI-1000 Ljubljana, Slovenia*
[g] *Santa Cruz Institute for Particle Physics (SCIPP), University of California, Santa Cruz, CA 95064, USA*
[h] *Department of Physics, Simon Fraser University, 8888 University Drive, Burnaby, B.C. V5A 1S6, Canada*
[i] *TRIUMF, 4004 Wesbrook Mall, Vancouver, B.C. V6T 2A3, Canada*
[j] *Institute of Pure and Applied Sciences, University of Tsukuba, 1-1-1 Tennodai, Tsukuba, Ibaraki 305-8571, Japan*
[k] *Department of Physics, University of Toronto, 60 Saint George St., Toronto, Ontario M5S1A7, Canada*
[l] *Institute of Particle and Nuclear Study, High Energy Accelerator Research Organization (KEK), 1-1 Oho, Tsukuba, Ibaraki 305-0801, Japan*

A R T I C L E I N F O

MSC:
82-06
82D37

Keywords:
HL-LHC
ATLAS ITk
Silicon micro-strip sensor
Polysilicon bias resistor
Testchip

A B S T R A C T

The high luminosity upgrade of the Large Hadron Collider, foreseen for 2029, requires the replacement of the ATLAS Inner Detector with a new all-silicon Inner Tracker (ITk). The expected ultimate total integrated luminosity of 4000 fb^{-1} means that the strip part of the ITk detector will be exposed to the total particle fluences and ionizing doses reaching the values of $1.6 \cdot 10^{15}\,\mathrm{MeV\,n_{eq}/cm^2}$ and 0.66 MGy, respectively, including a safety factor of 1.5. Radiation hard n^+-in-p micro-strip sensors were developed by the ATLAS ITk strip collaboration and are produced by Hamamatsu Photonics K.K. The active area of each ITk strip sensor is delimited by the n-implant bias ring, which is connected to each individual n^+ implant strip by a polysilicon bias resistor. The total resistance of the polysilicon bias resistor should be within a specified range to keep all the strips at the same potential, prevent the signal discharge through the grounded bias ring and avoid the readout noise increase. While the polysilicon is a ubiquitous semiconductor material, the fluence and temperature dependence of its resistance is not easily predictable, especially for the tracking detector with the operational temperature significantly below the values typical for commercial microelectronics.

Dependence of the resistance of polysilicon bias resistor on the temperature, as well as on the total delivered fluence and ionizing dose, was studied on the specially-designed test structures called ATLAS Testchips, both before and after their irradiation by protons, neutrons, and gammas to the maximal expected fluence and ionizing dose. The resistance has an atypical negative temperature dependence. It is different from silicon, which shows that the grain boundary has a significant contribution to the resistance. We discuss the contributions by parameterizing the activation energy of the polysilicon resistance as a function of the temperature for unirradiated and irradiated ATLAS Testchips.

1. Introduction

By 2026 the current ATLAS Inner Detector (ID) [1] will reach the end of its lifetime as it will not be able to cope with the harsh radiation environment, pile-up, occupancies and data transfer connected with the installation of the high luminosity upgrade of the Large Hadron Collider (HL-LHC). Thus, the ID will be replaced by a new all-silicon Inner Tracker (ITk) designed to withstand the high radiation damage associated with the anticipated ultimate total integrated luminosity of $4000\,\mathrm{fb}^{-1}$ accumulated during the expected operational time of more

* Corresponding author at: Academy of Sciences of the Czech Republic, Institute of Physics, Na Slovance 2, 18221 Prague 8, Czech Republic.
E-mail address: vera.latonova@cern.ch (V. Latoňová).

https://doi.org/10.1016/j.nima.2023.168119
Received 18 July 2022; Received in revised form 11 November 2022; Accepted 30 January 2023
Available online 10 February 2023

than 10 years [2]. The ITk will consist of two main parts — the pixel detector and the strip detector. For further purposes the strip detector is of our main interest. The total integrated luminosity of $4000\,\mathrm{fb}^{-1}$ means that the strip detector of the ITk will be exposed to the maximal total particle fluences of $1.6 \cdot 10^{15}$ 1 MeV $\mathrm{n_{eq}/cm^2}$ together with the total ionizing doses of 0.66 MGy including the safety factor of 1.5 and corresponding to the outermost End-cap disks and innermost ring [2]. For this purpose, radiation hard $\mathrm{n^+}$-in-p micro-strip sensors were developed by the ATLAS ITk strip collaboration and are manufactured by Hamamatsu Photonics K.K. [3]. The active area of the micro-strip sensor contains thousands of $\mathrm{n^+}$ implant strips, each of which is connected via the polysilicon bias resistor to the n-implant bias ring, running along the sensor's active area and keeping all strips on the same potential. The polysilicon resistors are designed with a high resistivity polysilicon process option. In ATLAS estimate, they have a surface resistivity of approximately $4\,\mathrm{k\Omega/square}$ and a tolerance, including the spread along the sensor, of $\pm 1.3\,\mathrm{k\Omega/square}$ [4].

Polysilicon, as the name implies, is a polycrystalline form of silicon comprising of many small randomly oriented crystallites (grains). The electrical properties of polysilicon are believed to be mostly determined by effects at the grain boundary, such as trapping and immobilization of charge carriers [5]. It is also assumed that the energy band structure known for single-crystalline silicon can be applied inside the individual crystallites. The temperature dependence of the polysilicon bias resistance and its activation energy are shown to be strongly depending on the doping concentration [5,6].

2. Irradiation and measurement procedure

The dependence of the resistance of polysilicon bias resistor on the temperature, as well as on the total delivered fluence and ionizing dose, was studied on 17 specially-designed test structures called ATLAS Testchips (Fig. 1(a)), which are fabricated on 6″ wafers together with MAIN sensors [7]. Each Testchip consists of several test structures providing the possibility to perform various tests such as the measurement of the polysilicon bias resistance (Fig. 1(b)). Individual testchips are identified by the batch and the wafer numbers, e.g. VPX32483-W00001.

14 samples were irradiated by protons, neutrons and gammas at different irradiation sites. The fluences were chosen to cover the maximal expected fluences in different parts of the strip detector (including the safety factor of 1.5) and the TID of 0.66 MGy corresponds to the maximal dose, which will be delivered to the End-cap part of the strip detector [2]. The gamma irradiation provides the cleanest test of TID effects, neutrons deliver the purest form of bulk damage and protons combine both of these effects.

In all cases, the samples were irradiated unbiased. The proton irradiation was performed at the University of Birmingham, UK [8] and at CYRIC, Japan [9]. The proton irradiation in Birmingham was performed by 27 MeV protons at a temperature of −27 °C. The maximal estimated uncertainty is 15 % of the fluence. At CYRIC the irradiation was performed by 70 MeV protons at a temperature of −15 °C with the maximal estimated uncertainty of 10 % of the fluence. Two samples were irradiated by reactor neutrons in Ljubljana, Slovenia at JSI TRIGA reactor [10] at a temperature of 40 °C with an estimated uncertainty of 10 % of the fluence. The gamma irradiation was achieved by ^{60}Co source at UJP Praha a.s., Czech Republic [11] at a temperature of 30 °C and an estimated uncertainty of 10 % of the TID. After the irradiation the samples were stored cold to prevent an uncontrolled annealing. Before the measurement, the irradiated Testchips were annealed for 80 min at 60 °C.

The remaining 3 samples were tested unirradiated, each at a different testing site.

The Testchips were measured in temperature range between −50 °C and +25 °C either wire-bonded on PCBs in an environmental chamber or placed on thermal chuck of a probe station and contacted by needles.

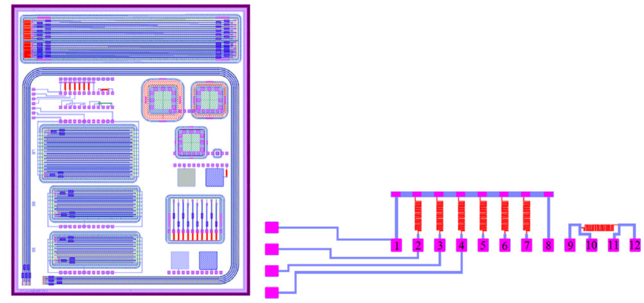

(a) An example of the ATLAS Testchip layout. (b) Detailed view of the bias resistors test structure layout.

Fig. 1. ATLAS Testchip and R_{bias} structure layout [7].

Regardless of whether the Testchip was wire-bonded or contacted by a needle, the testing procedure was the same. The pad '#1' (see Fig. 1(b)) was set to ground and consecutively the pads '#2' to '#4' were contacted and I-V scan was performed from −5 V to +5 V in 0.5 V steps. The bias resistance for each contacted pad is obtained from the I-V scans as $R_{\mathrm{bias,pad}} = \left(\frac{\mathrm{d}I}{\mathrm{d}V}\right)^{-1}$ [7]. For each temperature step the resulting bias resistance was calculated as an average of the bias resistances measured on the pads '#2' to '#4'.

3. Results I.: Temperature dependence and activation energy

Temperature dependence of R_{bias}. From the measured data it can be shown that the dependence of R_{bias} on temperature is exponential and can be thus described by the Eq. (1):

$$R_{\mathrm{bias}}(T) = R_0 \cdot \exp\left(\frac{E_a}{2kT}\right), \tag{1}$$

where E_a is the activation energy of polysilicon, k is the Boltzmann constant and R_0 is a scaling factor, which corresponds to $R_{\mathrm{bias}}(\infty)$.

The exponential dependence can be proven by displaying the measured data in Arrhenius-like plot (Fig. 2), in which we plot the logarithm of the ratio of R_{bias} and R_0 against reciprocal of the scaled temperature.

Activation energy of polysilicon. The fits of Arrhenius-like plots in Fig. 2 are linear with almost same slopes, which implies that the polysilicon bias resistance is characterized by a single activation energy. From the plot it is obvious that there are no random errors as the measured points of each sample perfectly correspond to the linear fit. However, we can see a systematic error between the measurements of the individual samples. Slight deviations in individual values of activation energies, which are visible as small differences in the slopes of the different lines, appear as the spread of the measured polysilicon bias resistance values due to systematic errors in the resistance measurement in different set-ups at different testing sites.[1] This spread of values was previously observed and published in [12] and [13].

The value of the activation energy for each sample was obtained by fitting the measured R_{bias} data using the logarithmization of Eq. (1): $\ln\left(\frac{R_{\mathrm{bias}}}{R_0}\right) = E_a \cdot \frac{1}{2kT}$. The results for different irradiation types are shown in Tables 1–4, from which it is obvious that the activation energy is independent of irradiation type. The small spread of the activation energy could indicate small variations in doping concentration, indicating high stability of the fabrication process. We attribute the lack of dependence on irradiation type to the very high doping concentration making the structure impervious to irradiation damages in the range studied.

[1] We estimate the temperature error of ±2 K, which affect the derivation of E_a little (≈ 1% around 0 °C).

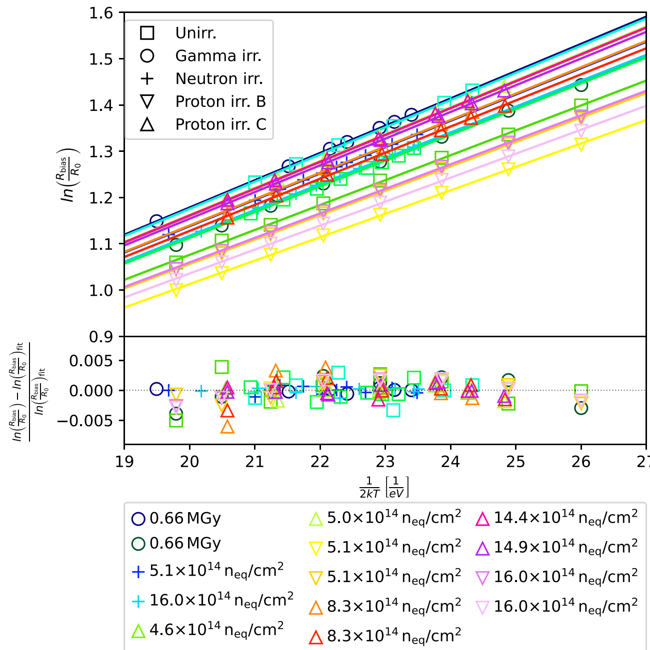

Fig. 2. The upper part of the plot shows Arrhenius-like plot of R_{bias} values vs temperature. The values for Testchips irradiated by different particles to various irradiation levels are denoted by markers and the corresponding linear fits are plotted as solid lines. The fitting function was obtained from the logarithmization of Eq. (1): $\ln\left(\frac{R_{\text{bias}}}{R_0}\right) = E_a \cdot \frac{1}{2kT}$. The lower part of the plot shows the difference between the measured and fitted values of R_{bias}.

Table 1
Activation energy (E_a) measured for unirradiated Testchips.

Testchip (Batch-Wafer)	$E_a[\cdot 10^{-3}\text{ eV}]$
VPX32483-W00001	58.7 ± 1.1
VPX33426-W00082	55.6 ± 0.9
VPX34148-W00201	53.8 ± 0.6

Table 2
Activation energy (E_a) measured for gamma irradiated Testchips.

Testchip (Batch-Wafer)	TID [MGy]	$E_a[\cdot 10^{-3}\text{ eV}]$
VPX32418-W00144	0.66 ± 0.07	58.9 ± 0.2
VPX33426-W00073	0.66 ± 0.07	55.7 ± 0.6

Table 3
Activation energy (E_a) measured for neutron irradiated Testchips.

Testchip (Batch-Wafer)	Fluence $[\cdot 10^{14}\ \text{n}_{\text{eq}}/\text{cm}^2]$	$E_a[\cdot 10^{-3}\text{ eV}]$
VPX32421-W00371	5.1 ± 0.5	56.9 ± 0.3
VPX32426-W00367	16.0 ± 1.2	55.9 ± 0.2

The activation energy of polysilicon was determined as the average value of the obtained activation energies:

$E_a^{\text{polysilicon}} = (55.8 \pm 0.1) \cdot 10^{-3}\text{ eV}.$

For a comparison, the activation energy of silicon is $E_a^{\text{silicon}} = 1.21\text{ eV}$, see [14]. The difference in these two values is in accordance with the assumption that the electrical properties of polysilicon are mostly determined by the effects at the grain boundary [5].

Table 4
Activation energy (E_a) measured for proton irradiated Testchips. The symbols ^{B} and ^{C} denote Testchips irradiated at Birmingham and at CYRIC, respectively.

Testchip (Batch-Wafer)	Fluence $[\cdot 10^{14}\ \text{n}_{\text{eq}}/\text{cm}^2]$	$E_a[\cdot 10^{-3}\text{ eV}]$
VPX32423-W80366^C	4.6 ± 0.5	58.0 ± 0.2
VPX32587-W00064^C	5.0 ± 0.5	58.1 ± 0.6
VPA37915-W00314^B	5.1 ± 0.8	50.6 ± 0.3
VPA37915-W00306^B	5.1 ± 0.8	52.8 ± 0.4
VPA37915-W00295^C	8.3 ± 0.8	57.0 ± 1.4
VPX37425-W00755^C	8.3 ± 0.8	56.4 ± 0.6
VPX32425-W00317^C	14.4 ± 1.4	58.1 ± 0.5
VPX32471-W00051^C	14.9 ± 1.5	57.7 ± 0.3
VPA37915-W00333^B	16.0 ± 2.4	53.0 ± 0.4
VPA37915-W00340^B	16.0 ± 2.4	51.8 ± 0.4

4. Prediction of temperature development of R_{bias} for various irradiations

In the previous section it has been shown that the temperature dependence of R_{bias} can be described by Eq. (1) and that the activation energy as a material constant has the same value for all samples. Now, we will derive a common function for all samples that will describe the temperature evolution of R_{bias} for each sample based on just one reference value $R_m = R_{\text{bias}}(T_m)$ measured at the temperature T_m for the particular sample.

For a general sample we set $R_m = R_{\text{bias}}(T_m)$ at a temperature T_m. Then, from Eq. (1) we get for R_0 relation (2):

$$R_0 = \frac{R_m}{\exp\left(\frac{E_a}{2kT_m}\right)}. \tag{2}$$

By inserting Eq. (2) into Eq. (1) we obtain for all other samples:

$$\begin{aligned} R(T; T_m, R_m) &= \frac{R_m}{\exp\left(\frac{E_a}{2kT_m}\right)} \exp\left(\frac{E_a}{2kT}\right) \\ &= R_m(T_m) \cdot \exp\left(\frac{E_a}{2k}\left(\frac{1}{T} - \frac{1}{T_m}\right)\right). \end{aligned} \tag{3}$$

Using the derived formula, we can compare the measured R_{bias} values of each Testchip with the curve obtained from Eq. (3), where we used as R_m for each sample its bias resistance value at temperature $T_m = 253.15\text{ K}$ and for the activation energy we used the value $E_a = 53.8 \cdot 10^{-3}\text{ eV}$ obtained from the fit for one of the unirradiated Testchips.

The results are shown in Fig. 3. The upper part of the plot shows the comparison between the measured values of R_{bias} with the curves obtained from Eq. (3). The lower part of the plot shows the difference between the real measured R_{bias} values and the predicted values of R_{bias} from Eq. (3) (noted as R_{model}) for each Testchip expressed at every temperature value. It can be shown that in the middle of the temperature range the R_{model} values obtained from Eq. (3) match very well with the measured results. At both ends of the temperature range the discrepancies between the model and real values become more apparent, however still relatively small ($< 2\,\%$).

5. Results II.: Dependence of R_{bias} on Total Ionizing Dose (TID) and fluence

R_{bias} *Vs fluence.* The fluence dependence of the R_{bias} values measured for samples irradiated by protons and neutrons is shown in Fig. 4. Neglecting the slight span in individual measured values, which is present already for unirradiated samples and is in accordance with [12], we do not see any correlation between the measured R_{bias} values and fluence for protons or neutrons.

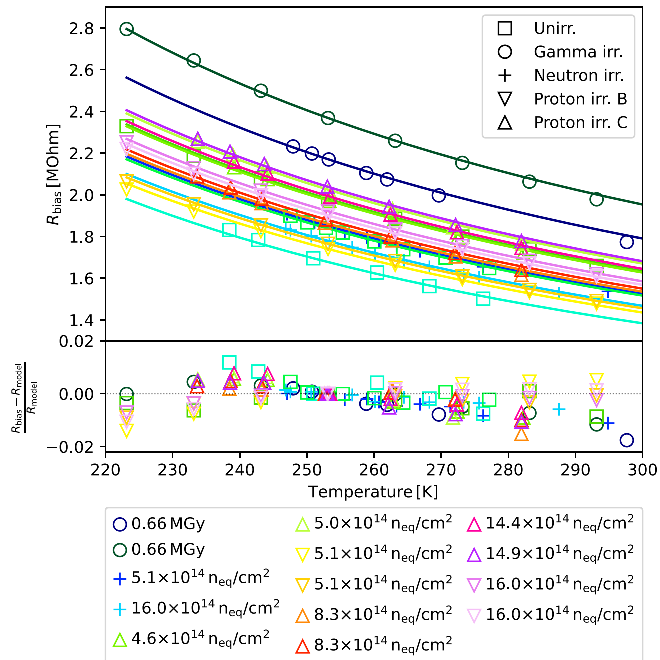

Fig. 3. The upper part of the plot shows the calculated temperature dependence of R_{bias} (solid lines) compared with the measured R_{bias} values (markers). The lower part of the plot shows the difference between the real measured R_{bias} values and the predicted values of R_{bias} from Eq. (3) (noted as R_{model}) for each temperature value.

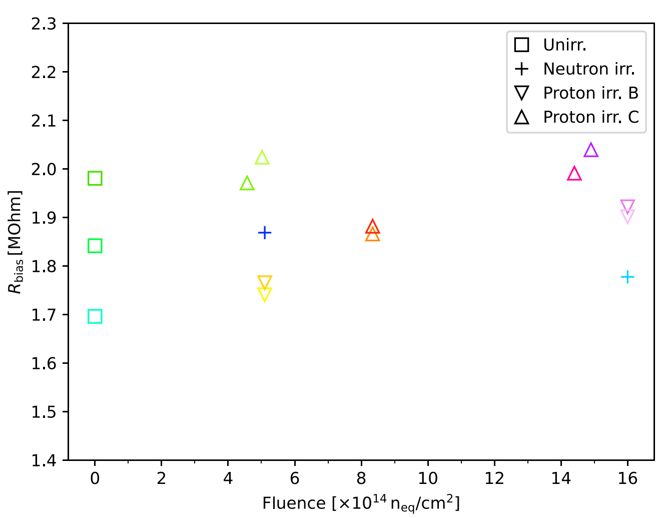

Fig. 4. Dependence of R_{bias} measured at −20 °C on fluence.

In Fig. 5 the ratio of two R_{bias} values of the same sample measured at temperatures −20 °C and −10 °C vs the total delivered fluence is plotted.

R_{bias} Vs TID. In order to study the dependence of R_{bias} on TID it was necessary to convert the proton and neutron fluence into TID. The proton irradiation was converted to TID using the formula (4):

$$\mathrm{TID} = \frac{\Phi}{\kappa}\left(\frac{\mathrm{d}E}{\mathrm{d}x}\right)_{E_p}, \tag{4}$$

where Φ is the proton fluence in 1 MeV neutron equivalent, $\left(\frac{\mathrm{d}E}{\mathrm{d}x}\right)_{E_p}$ is the stopping power of protons with energy E_p in silicon taken from Ref. [15] and κ is the hardness factor (κ is 1.552 and 2.2 for CYRIC and Birmingham, respectively). The TID in neutron irradiated Testchips caused by secondary particles has been assessed to be 1 kGy per $1 \cdot 10^{14}\ \mathrm{n_{eq}/cm^2}$. The dependence of R_{bias} on TID is presented in Fig. 6, where we do not observe any significant change of R_{bias} with TID for samples irradiated by protons and neutrons. We can see that R_{bias} values after gamma irradiation are higher in comparison to the values obtained after proton and neutron irradiation. This effect was observed for tens of gamma irradiated Testchips, which were tested during pre-production and production as a part of Quality Assurance procedure and the results were compared to the proton and neutron irradiated Testchips and presented in [13]. The source of the slightly higher R_{bias} values in case of gamma irradiated Testchips is under investigation.

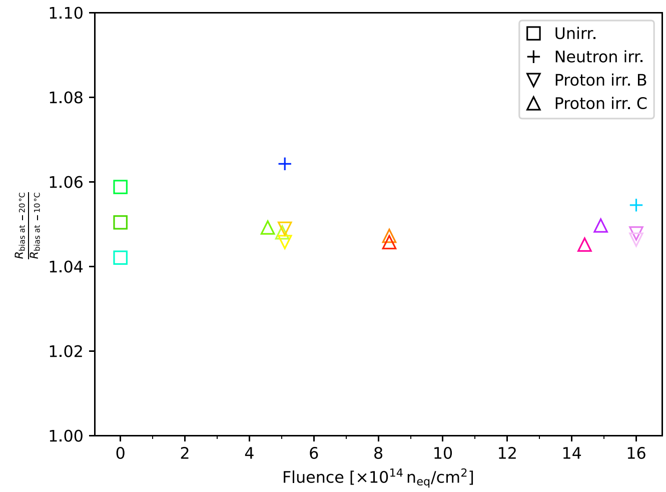

Fig. 5. Ratio of two R_{bias} values of the same sample measured at temperatures −20 °C and −10 °C vs fluence.

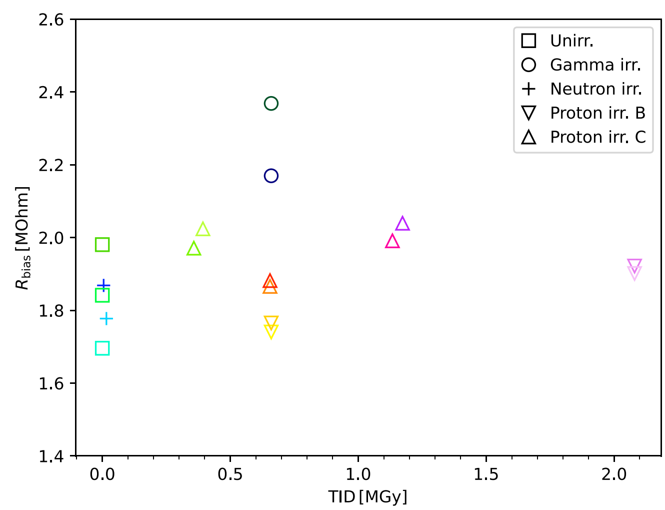

Fig. 6. Dependence of R_{bias} measured at −20 °C on TID.

Fig. 7 shows the ratio of two R_{bias} values of the same sample at temperatures −20 °C and −10 °C, from which it is apparent that the activation energy does not change with irradiation.

6. Conclusions

Dependence of the resistance of polysilicon bias resistor on temperature and irradiation was studied on several ATLAS ITk Testchips that were specially designed to have the same properties as the large-format micro-strip sensors, which will be installed in the ATLAS ITk detector in HL-LHC.

It has been shown that the value of polysilicon bias resistance decreases as $\exp\left(\frac{E_a}{2kT}\right)$ with temperature. By fitting the values of R_{bias} measured at different temperatures by the Formula (1) it is possible to

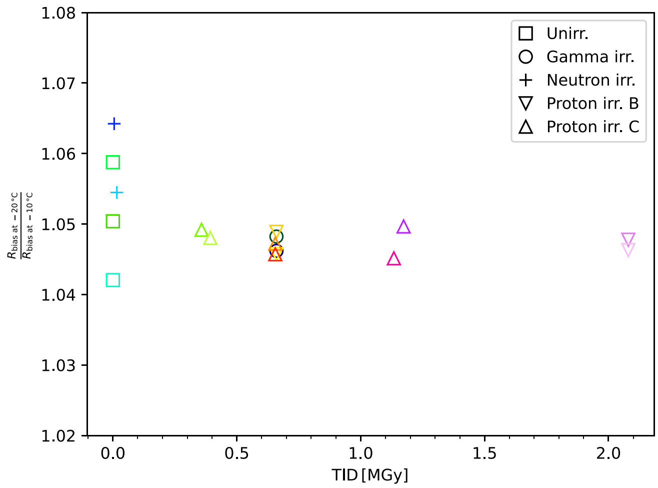

Fig. 7. Ratio of two R_{bias} values of the same sample at temperatures −20 °C and −10 °C vs TID.

extract the activation energy for each sample. We determined an average activation energy of polysilicon as $E_a^{\mathrm{polysilicon}} = (55.8 \pm 0.1) \cdot 10^{-3}$ eV, which differs from the activation energy of single-crystalline silicon (1.21 eV) and thus implies that the electrical properties of polysilicon are governed as it was assumed. The activation energy is shown to be independent from samples and irradiation types.

Further, by using Eq. (3), it was possible to determine the temperature evolution of R_{bias} for any studied sample based on one value of bias resistance R_m measured for this sample at a temperature T_m. This result was verified in Fig. 3, where it was also shown that this model matches very well the values in the middle of the studied temperature range, i.e. from −50 °C to +25 °C. Even at the edges of the temperature range, the discrepancies are quite small (< 2 %).

It has been also shown that for neutron and proton irradiation, the value of R_{bias} at a given temperature does not change with fluence or TID. After gamma irradiation the R_{bias} value is slightly higher compared to unirradiated samples or samples irradiated by protons and neutrons, which is in accordance with [13]. From Figs. 4 to 7 it is obvious that R_{bias} does not depend on the type and level of irradiation.

Declaration of competing interest

The authors declare that they have no known competing financial interests or personal relationships that could have appeared to influence the work reported in this paper.

Acknowledgments

This work was supported by the Ministry of Education, Youth and Sports of the Czech Republic via the projects LTT17018 Inter-Excellence and LM2018104 CERN-CZ, Charles University, Czech Republic grant GAUK 942119, the Slovenian Research Agency (research core funding No. P1_0135), the Canada Foundation for Innovation and the Natural Sciences and Engineering Research Council of Canada, the US Department of Energy, grant DE-SC0010107, JSPS, Japan Grant-in-Aid for Research Activity Start-up 20K22346 and the Spanish R&D grant PID2019-110189RB-C22, funded by MCIN/ AEI/10.13039/5011000 11033. The authors would like to thank the crew at the TRIGA reactor in Ljubljana and gamma irradiation facility UJP Praha a.s. for help with the irradiation of the detectors.

References

[1] The ATLAS Collaboration, et al., The ATLAS experiment at the CERN large hadron collider, J. Instrum. 3 (08) (2008) S08003, http://dx.doi.org/10.1088/1748-0221/3/08/s08003.

[2] ATLAS Collaboration, Technical Design Report for the ATLAS Inner Tracker Strip Detector, Tech. Rep. CERN-LHCC-2017-005. ATLAS-TDR-025, CERN, Geneva, 2017, https://cds.cern.ch/record/2257755.

[3] Y. Unno, et al., ATLAS17LS – A large-format prototype silicon strip sensor for long-strip barrel section of ATLAS ITk strip detector, Nucl. Instrum. Methods Phys. Res. A 989 (2021) 164928, http://dx.doi.org/10.1016/j.nima.2020.164928.

[4] Y. Unno, et al., Specifications and pre-production of n⁺-in-p large-format strip sensors fabricated in 6-inch silicon wafers, ATLAS18, for inner tracker of ATLAS detector for high-luminosity large hadron collider, J. Instrum.(Preprint No. JINST_002T_1022) (2022) Accepted for Publication.

[5] J.Y.W. Seto, The electrical properties of polycrystalline silicon films, J. Appl. Phys. 46 (1975) 5247–5254, http://dx.doi.org/10.1063/1.321593.

[6] H. Muro, et al., Determination of Electrical Properties of n-Type and p-Type Polycrystalline Silicon Thin Films as Sensor Materials, Sens. Mater. 18 (2006) 433–444.

[7] M. Ullán, et al., Quality assurance methodology for the ATLAS inner tracker strip sensor production, Nucl. Instrum. Methods Phys. Res. A 981 (2020) 164521, http://dx.doi.org/10.1016/j.nima.2020.164521.

[8] P. Allport, et al., Recent results and experience with the birmingham MC40 irradiation facility, J. Instrum. 12 (03) (2017) C03075, http://dx.doi.org/10.1088/1748-0221/12/03/c03075.

[9] K. Nakamura, et al., Irradiation and testbeam of KEK/HPK planar p-type pixel modules for HL-LHC, J. Instrum. 10 (06) (2015) C06008, http://dx.doi.org/10.1088/1748-0221/10/06/c06008.

[10] L. Snoj, et al., Radiation hardness studies and detector characterisation at the JSI TRIGA reactor, EPJ Web Conf. 225 (2020) 04031, http://dx.doi.org/10.1051/epjconf/202022504031.

[11] UJP PRAHA a.s., 2022, https://ujp.cz/en/. ((Accessed on 13 May 2022)).

[12] P. Allport, et al., Pre-Production Results from ATLAS ITk Strip Sensors Quality Assurance Testchip, J. Instrum. 17 (11) (2022) C11002, http://dx.doi.org/10.1088/1748-0221/17/11/C11002.

[13] S. Hirose, et al., ATLAS ITk strip sensor quality assurance tests and results of ATLAS18 pre-production sensors, in: Poster on the 31 st International Workshop on Vertex Detectors. The proceedings will be published online in JPS Conference Proceedings, 2022, (ISSN 2435-3892) https://indico.cern.ch/event/1140707/contributions/5002363/.

[14] A. Chilingarov, Temperature dependence of the current generated in Si bulk, J. Instrum. 8 (10) (2013) P10003, http://dx.doi.org/10.1088/1748-0221/8/10/p10003.

[15] Stopping power and range tables for protons, 2022, https://physics.nist.gov/cgi-bin/Star/ap_table.pl. (Accessed on 13 May 2022).